ELECTROMAGNETIC SCATTERING BY ARBITRARILY SHAPED TWO-DIMENSIONAL PERFECTLY CONDUCTING OBJECTS COATED WITH HOMOGENEOUS ANISOTROPIC MATERIALS

Benjamin Beker, *Department of Electrical Computer Engineering, University of South Carolina, Columbia, South Carolina 29208, USA*

Korada R. Umashankar, *Department of Electrical Engineering and Computer Science, University of Illinois at Chicago, Chicago, Illinois 60680, USA*

Allen Taflove, *Department of Electrical Engineering and Computer Science, McCormick School of Engineering, Northwestern University, Evanston, Illinois 60208, USA*

ABSTRACT

Combined-field surface integral equations are applied to analyze electromagnetic scattering from coated perfectly conducting objects. The conducting core and the homogeneous anisotropic coating layers covering it are assumed to be two-dimensional and of arbitrary shape. Furthermore, individual layers of anisotropic material constituting the composite clad structure are allowed to have distinct medium tensor properties. Numerical solution of the resulting integral equations is facilitated by the method of moments. Equivalent surface currents on the metal core and the jacket surface are computed, and along with the corresponding radar cross section are presented for a variety of scattering geometries.

1. INTRODUCTION

Scattering by homogeneous anisotropic objects has attracted a great deal of interest in recent years. Numerical methods based on integral [1]-[6] as well as differential [7] equations have been employed to analyze this problem. Although the research effort in the past was primarily concentrated on two-dimensional (2-D) geometries, some progress has been made in the analysis of three-dimensional (3-D) anisotropic scatterers [6], [8] as well. In two-dimensions, for bulk anisotropic objects a good amount of work has already been done. While volumetric integral equations, (VIEs), were used to analyze electromagnetic scattering properties of circular as well as elliptic cylinders [1], [2], variational methods were considered for the treatment of more general shapes, such as the square cylinder [3]. However, both the variational and VIE formulations were restricted to objects with small electrical dimensions.

More recently, to overcome size limitations, surface integral equations were developed to allow for the treatment of anisotropic scatterers whose dimensions are nearing the resonant region, and in some cases even extend beyond it. Particularly, a combined-field surface integral equation or the CFSIE approach was found to be very useful for the numerical analysis of such problems [4]-[6]. This method is very similar to that which is most commonly applied to isotropic scatterers [9]. It is based on the potential representation of electromagnetic (EM)

Electromagnetics 10:387-406, 1990

fields in the anisotropic region with the equivalence principle invoked to obtain the integral equations for the unknown equivalent surface currents. The most attractive feature of this method is its natural ability to treat scatterers with arbitrary geometrical shapes. The applicability of the CFSIE approach to solve boundary-value problems involving bulk anisotropic objects was already demonstrated by computing the equivalent surface currents and the corresponding radar cross sections (RCS) for a variety of scattering geometries [4], [5].

The numerical flexibility of CFSIEs is offered by the nature of the formulation, since integration is confined to object's surface only; whereas for volumetric methods, the integration must be performed throughout entire volume of the scatterer. Of course, there is a limit imposed by object's size, for which the surface formulation to EM scattering is no longer computationally efficient. But nonetheless, for scatterers with reasonable dimensions, the CFSIE approach will lend itself as a more effective tool in the numerical analysis of such problems than VIEs or variational techniques.

In addition to the CFSIEs, yet another surface formulation, has recently become available [10]. As opposed to the potential representation of the electromagnetic field inside the homogeneous anisotropic region, the method of [10] is based on integral equations for the fields themselves. Numerical implementation of this approach to the solution of the scattering problem has also been employed in calculations of the RCS for bulk anisotropic objects bounded by smooth as well as discontinuous contours.

In contrast to the integral equation methodologies, numerical approaches based on differential equations have also been considered for isotropic [7] as well as anisotropic objects [5]. The most popular of the available techniques is the Finite-Difference Time-Domain, (FD-TD), approach. It has been used extensively for comparison purposes in conjunction with the CFSIEs in the past, [5], and will be used herein for anisotropically coated arbitrarily shaped objects as well.

Theoretical as well as the numerical treatment of anisotropically coated metallic objects, thus far, has been primarily restricted to two-dimensions [11]-[13]. However, even for the 2-D case no comprehensive effort dealing with composite structures of arbitrary shapes and medium parameters has been performed to date. The work presented in [11] is limited to a special class of composite scatterers only. The objects consist of a perfectly conducting circular cylinder and a number of coaxial circular anisotropic layers separated by intermediate isotropic regions. The anisotropic layers are very thin, thereby allowing for great simplifications in the analytical formulation. Specifically, in the modal solution of the problem, anisotropic layers are accounted for by using jump impedance boundary conditions.

A somewhat more general case of the coated structure, as compared to that analyzed in [11], is treated in [12]. Therein, the circular metallic core is surrounded by a single annular layer of biaxial material having a finite thickness. In addition to this shield, an impedance sheet is also placed over the anisotropic jacket. The scattered fields from the overall composite structure are obtained by using a modal solution to the boundary-value problem.

Finally, the surface method proposed in [10] was also used in treating the coated object problem, and in particular to calculate its RCS [13]. Although the formulation, developed in [10], apparently is applicable to anisotropic media with arbitrary invertible tensors, for coated objects it was reduced and numerically implemented for shielding structures with rotationally invariant (gyrotropic-type) materials [13]. That is, both $\underline{\underline{\varepsilon}}$ and $\underline{\underline{\mu}}$ were now assumed as skew-symmetric, in addition to having two of their transverse diagonal elements equal to one another, thereby simplifying the scattering problem significantly.

In this paper, scattering by objects consisting of a metallic core covered by a number of layers of homogeneous anisotropic material is considered. Their two-dimensional shapes are assumed to be arbitrary and may contain surface discontinuities. The numerical analysis is based on the combined-field surface integral equations (CFSIEs). Two variations of the formulation will be presented, and the advantages of each will briefly be discussed. One will deal with CFSIEs in which the Lorentz gauge condition is used to eliminate the scalar potential, whereas the other will focus on the mixed potential formulation, wherein both scalar and vector potentials are retained in the resulting integral equations. However, the emphasis of the paper is on the versatility of the CFSIEs and the numerical results which will be calculated using them for various geometries of anisotropically coated metallic objects. Equivalent surface currents, often excluded from previous studies, and the corresponding RCS patterns will be computed and presented for coated circular, elliptic, and square cylinders which presently are unavailable elsewhere in the literature.

2. INTEGRAL EQUATIONS FOR COATED 2-D SCATTERERS

The electromagnetic field in an infinite two-dimensional ($\partial/\partial z \rightarrow 0$) homogeneous anisotropic medium occupying region *i* and characterized by $\underline{\underline{\varepsilon}}_i$ and $\underline{\underline{\mu}}_i$ may be decomposed into its TE (Transverse Electric) and TM (Transverse magnetic) parts [4]. For such problems, duality is applicable in determining the fields for one polarization (TE) whenever their representations for the other polarization (TM) are known [4]. As a result, the detailed portion of the ensuing development will be restricted to the TM polarization, while for the TE case, discussion will be brief, highlighting just the principles invoked to find the corresponding CFSIE set.

2.1 TM Scattering

According to [4], for the TM case, expressions for the nonzero field components in terms of vector and scalar potentials which have been derived earlier, [4], are given by

$$E_{zi}(r) = -j\omega A_{zi}(\mathbf{J}_i) - \mathbf{a}_z \cdot (\underline{\underline{\varepsilon}}_i)^{-1} \cdot (\nabla \times \mathbf{F}_i(\mathbf{M}_i))/\varepsilon_o \quad (1)$$

$$\mathbf{H}_i(r) = -j\omega \mathbf{F}_i(\mathbf{M}_i) - \nabla \psi_i(\mathbf{M}_i) + (\underline{\underline{\mu}}_i)^{-1} \cdot (\nabla \times \mathbf{A}_i(\mathbf{J}_i))/\mu_o \quad (2)$$

It is clear that in equations (1) and (2), the currents $\mathbf{J}_i = J_{zi}\mathbf{a}_z$ and $\mathbf{M}_i = M_{si}\mathbf{a}_s$ act as the sources for the potentials and consequently for the fields E_{zi} and $\mathbf{H}_i$. The integral expressions for A_{zi}, ψ_i, and $\mathbf{F}_i$ were previously obtained from Helmholtz

equations which they satisfy [4], and are restated below for the sake of completeness

$$A_{zi}(r) = \mu_o/4j \int_{C_i} \gamma_{mi} (\mu_{xx}\mu_{yy})_i^{-1/2} J_{zi}(r') \left(H_o^{(2)}(k_{ami}R_{mi}) \right) ds' \quad (3)$$

$$\mathbf{F}_i(r) = (\varepsilon_o\varepsilon_{zz})_i/4j \int_{C_i} \gamma_{mi} (\mu_{xx}\mu_{yy})_i^{-1/2} \left(\underline{\underline{\mu}}_i^{-1} \cdot \mathbf{M}_i(r') \right) \left(H_o^{(2)}(k_{ami}R_{mi}) \right) ds' \quad (4)$$

$$\psi_i(r) = 1/(j4\mu_o) \int_{C_i} (\mu_{xx}\mu_{yy})_i^{-1/2} \rho_i^m(r') \left(H_o^{(2)}(k_{ami}R_{mi}) \right) ds' \quad , \quad (5)$$

where, of course, the charge density, ρ^m in equation (5), is related to **M** via the continuity equation. The remaining parameters k_{ami} and R_{mi} appearing in (3) through (5) are defined as

$$k^2_{ami} = k_o^2 (\varepsilon_{zz})_i \gamma_{mi} = k^2_o (\varepsilon_{zz})_i (\mu_{xx}\mu_{yy} + \mu_{xy}^2)_i \quad (6)$$

$$R^2_{mi} = (x - x')^2/(\mu_{xx})_i + (y - y')^2/(\mu_{yy})_i \quad (7)$$

with the permittivity and the permeability tensors of the medium $(\underline{\underline{\varepsilon}})_i$ and $(\underline{\underline{\mu}})_i$ given by the following relations

$$(\underline{\underline{\varepsilon}})_i = \begin{vmatrix} \varepsilon_{xx} & \varepsilon_{xy} & 0 \\ -\varepsilon_{xy} & \varepsilon_{yy} & 0 \\ 0 & 0 & \varepsilon_{zz} \end{vmatrix} \qquad (\underline{\underline{\mu}})_i = \begin{vmatrix} \mu_{xx} & \mu_{xy} & 0 \\ -\mu_{xy} & \mu_{yy} & 0 \\ 0 & 0 & \mu_{zz} \end{vmatrix} . \quad (8)$$

While the most general, anisotropic medium, would be described by tensors with $\alpha_{yx} \neq -\alpha_{xy}$, where α may be taken as any element of either $\underline{\underline{\varepsilon}}$ or $\underline{\underline{\mu}}$, the skew-symmetric nature of the permittivity and permeability will, nonetheless, still represent a wide array of physically realizable media. Whenever the diagonal elements of $\underline{\underline{\varepsilon}}$ and $\underline{\underline{\mu}}$ are real, and at the same time, the off-diagonal terms are purely imaginary, these tensors are Hermitian. And in addition, if either μ_{xx} is equal μ_{yy} or ε_{xx} is equal ε_{yy}, then $\underline{\underline{\mu}}$ and $\underline{\underline{\varepsilon}}$ will correspond to Ferrites or Plasmas, respectively [14]. Furthermore, for such tensors, if elements α_{xy} and α_{yx} are also real, but negatives of one another, they will depict rotationally invariant media treated in [13], which is just a special case of the formulation discussed herein.

Equations (8) are also capable of describing, yet another, important class of anisotropic media. Uniaxial and biaxial materials, having their principal axes aligned with the coordinate axes of the scatterer geometry, are characterized by permittivity and permeability tensors whose off-diagonal terms are zero. Therefore, the skew-symmetric forms of $\underline{\underline{\varepsilon}}$ and $\underline{\underline{\mu}}$, as given by equation (8), are not intended to represent any specific medium, but rather they provide for a conveniently compact mathematical description encompassing a wide variety of media which may be treated by the CFSIE method.

In order to obtain another, but equally valid, representation for the magnetic field inside the medium, the Lorentz gauge condition, $(j\omega \nabla \cdot (\underline{\underline{\mu}}_i \cdot \mathbf{F}_i) = k^2_{ami} \psi_i)$, may be employed to eliminate the scalar potential ψ_i from equation (2). This,

subsequently, will allow for the *H*-field integral equation to be rewritten in terms of vector potentials alone, i. e.,

$$\mathbf{H}_i(r) = - j\omega\mathbf{F}_i(\mathbf{M}_i) - j\omega\nabla (\nabla \cdot (\underline{\underline{\mu}}_i \cdot \mathbf{F}_i(\mathbf{M}_i))/k^2_{ami}) + (\underline{\underline{\mu}}_i)^{-1} \cdot (\nabla \times \mathbf{A}_i(\mathbf{J}_i))/\mu_o \quad (9)$$

and now, along with the companion equation for the electric field, relation (9) may serve as an alternative in representating the EM field inside the homogeneous anisotropic region. This action may be warranted for situations, wherein derivatives of the current density (i. e., the charge) in the numerical solution of the CFSIEs most often are avoided. Such applications will appear in practice whenever Pocklington-type integral equations must be solved, as for example, in the analysis EM coupling to wires throught narrow slots in perfectly conducting screens, [15], or other kinds of apertures [16]. Discussion regarding the advantages and disadvantages of the two formulations (vector vs. mixed potential) outlined above, as they pertain to the anisotropic medium, will be expanded and will be presented later in conjunction with the calculated results.

Consider now a boundary-value problem consisting of a perfectly conducting object coated with several layers of anisotropic material. As illustrated in Fig. 1, the core as well as each anisotropic layer may be arbitrarily shaped and have distinct medium properties. Moreover, the composite structure is also assumed to be excited by a TM-polarized, normally incident, plane wave. Then according to [4] and the preceding discussion, under such conditions the fields in region *i* due to equivalent currents $\mathbf{J}_i$ and $\mathbf{M}_i$ are given by equations (1) and (2) or (1) and (9), wherein the subscript attached to the potential denotes the appropriate Green's function of the medium which occupies the subspace *i*. And correspondingly, the subscripts on **J** or **M** will point to the location of the boundary contour where these equivalent currents are assumed to flow. The integral expressions for the potentials A_{zi}, $\mathbf{F}_i$, and ψ_i appearing in (1) and (9) were earlier defined for region *i* through the relations (3), (4), and (5).

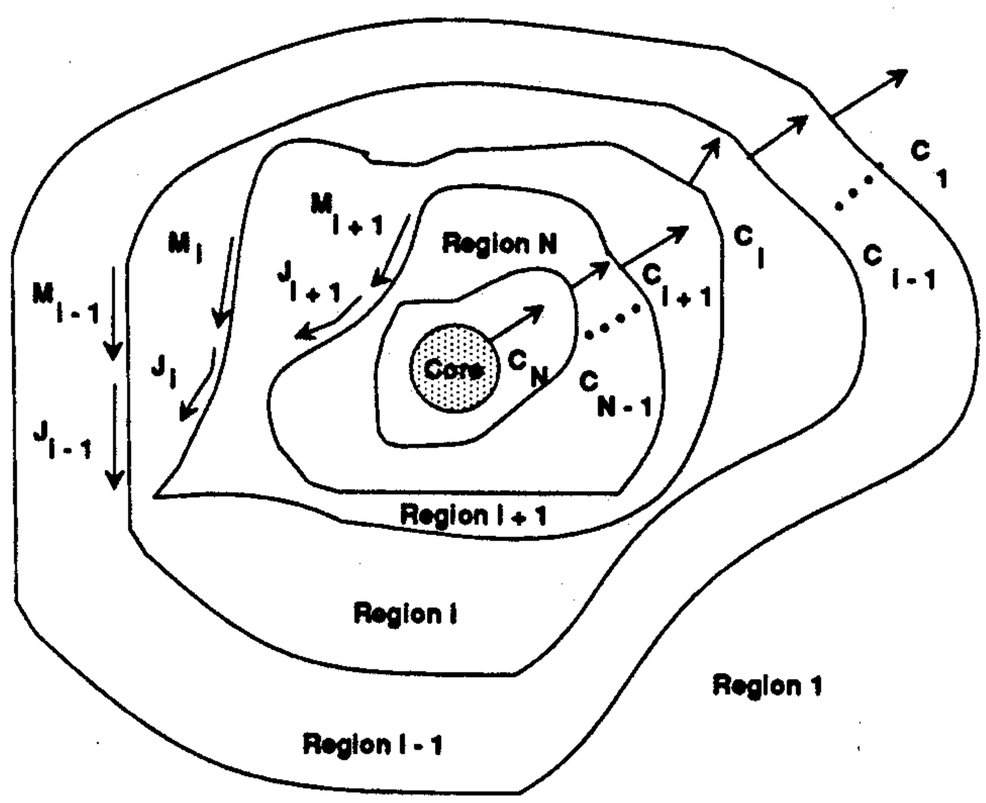

FIGURE 1: Geometry of an arbitrarily shaped coated metallic scatterer

Notice however, that equations (1) and (2) will only partially contribute to total fields (E_{zi}^T and $\mathbf{H}_i^T$) within the space enclosed by contours C_{i-1} and C_i. The currents $\mathbf{J}_{i-1}$ and $\mathbf{M}_{i-1}$, which influence the E_{zi}^T and $\mathbf{H}_i^T$ therein as well, will provide for the remaining contributions to the total fields. But to enforce the boundary conditions at the interface C_i, the total fields setup within the region *i+1* will also be required. From Fig. 1 it is quite clear that surface currents $\mathbf{J}_i$, $\mathbf{M}_i$ and $\mathbf{J}_{i+1}$, $\mathbf{M}_{i+1}$ will be responsible for giving rise to E_{zi+1}^T and $\mathbf{H}_{i+1}^T$ inside this region, with integral expressions for these fields obtained from (1) and (2) by using an appropriate substitution of the subscripts.

The continuity of the tangential components of **E** and **H** across the contour C_i will lead to two equations for currents ($\mathbf{J}_i$, $\mathbf{M}_i$), ($\mathbf{J}_{i+1}$, $\mathbf{M}_{i+1}$), and ($\mathbf{J}_{i-1}$, $\mathbf{M}_{i-1}$) at this interface, namely to

$$0 = \{ - [E_{zi}(\mathbf{J}_i , \mathbf{M}_i) + E_{zi+1}(\mathbf{J}_i , \mathbf{M}_i)] + [E_{zi}(\mathbf{J}_{i-1} , \mathbf{M}_{i-1})]$$

$$+ [E_{zi+1}(\mathbf{J}_{i+1} , \mathbf{M}_{i+1})] \}_{Ci} \qquad (10)$$

and

$$0 = \mathbf{a}_{ni} \times \{ - [\mathbf{H}_i(\mathbf{J}_i , \mathbf{M}_i) + \mathbf{H}_{i+1}(\mathbf{J}_i , \mathbf{M}_i)] + [\mathbf{H}_i(\mathbf{J}_{i-1} , \mathbf{M}_{i-1})]$$

$$+ [\mathbf{H}_{i+1}(\mathbf{J}_{i+1} , \mathbf{M}_{i+1})] \}_{Ci} \ , \qquad (11)$$

with $\mathbf{a}_{ni}$ denoting an outward pointing unit normal to C_i. In the same manner, boundary conditions at all other internal interfaces, i = 2, ... , N-1, separating any two individual anisotropic coating sheets may be imposed as well. But for the ambient medium and the first external anisotropic layer (i = 2), equations (10) and (11) must now be modified to take into account the excitation as well as isotropic properties of the free-space. This may be readily achieved by letting in above equations for $\mathbf{J}_{i-1}$ and $\mathbf{M}_{i-1}$ to act as sources for the incident field, i. e., $\mathbf{J}_s$ and $\mathbf{M}_s$, and in addition, for the free-space, equations (3) through (5) must also be adjusted to allow for $\underline{\underline{\varepsilon}}_1 \rightarrow \varepsilon_1$ and $\underline{\underline{\mu}}_1 \rightarrow \mu_1$. In other words, for the outermost boundary (C_1) separating two distinct media (e. g., regions 1 and 2 as illustrated in Fig. 1), the following set of equations is obtained for $\mathbf{J}_1$ and $\mathbf{M}_1$ flowing on contour C_1:

$$- E^i_{z1} = -j\omega (A_{z1} + A_{z2}) - \mathbf{a}_z \cdot \{ (\nabla \times \mathbf{F}_1)/\varepsilon_o\varepsilon_1 + (\underline{\underline{\varepsilon}}_2)^{-1} \cdot (\nabla \times \mathbf{F}_2)/\varepsilon_o \} \qquad (12)$$

$$- \mathbf{a}_n \times \mathbf{H}^i_1 = - \mathbf{a}_n \times \{ j\omega(\mathbf{F}_1 + \mathbf{F}_2) + \nabla (\psi_1 + \psi_2) \} + \mathbf{a}_n \times \{ (\nabla \times \mathbf{A}_1)/\mu_o\mu_1 +$$

$$+ (\underline{\underline{\mu}}_2)^{-1} \cdot (\nabla \times \mathbf{A}_2)/\mu_o \} \qquad . \quad (13)$$

where subscripts on the potentials will once again refer to the appropriate Green's function of the medium. Note also that the incident fields E^i_{z1} and $\mathbf{H}^i_1$, assumed to exist in region 1, are now included in both expressions (12) and (13).

Next, in the method of moments solution, the unknown equivalent currents J_{z1} and M_{s1} as usual will be expanded in terms of staggered weighted pulse functions as shown in Fig. 2. The same set of basis functions will subsequently be employed to test equations (12) and (13), thereby providing desired matrix equations for

contour C_1. But if the problem involves more than a single boundary, such as for the coated scatterer, then the procedure outlined for interface C_1 may be repeated for every other interface to obtain the required matrix equations for the equivalent currents on all remaining contours.

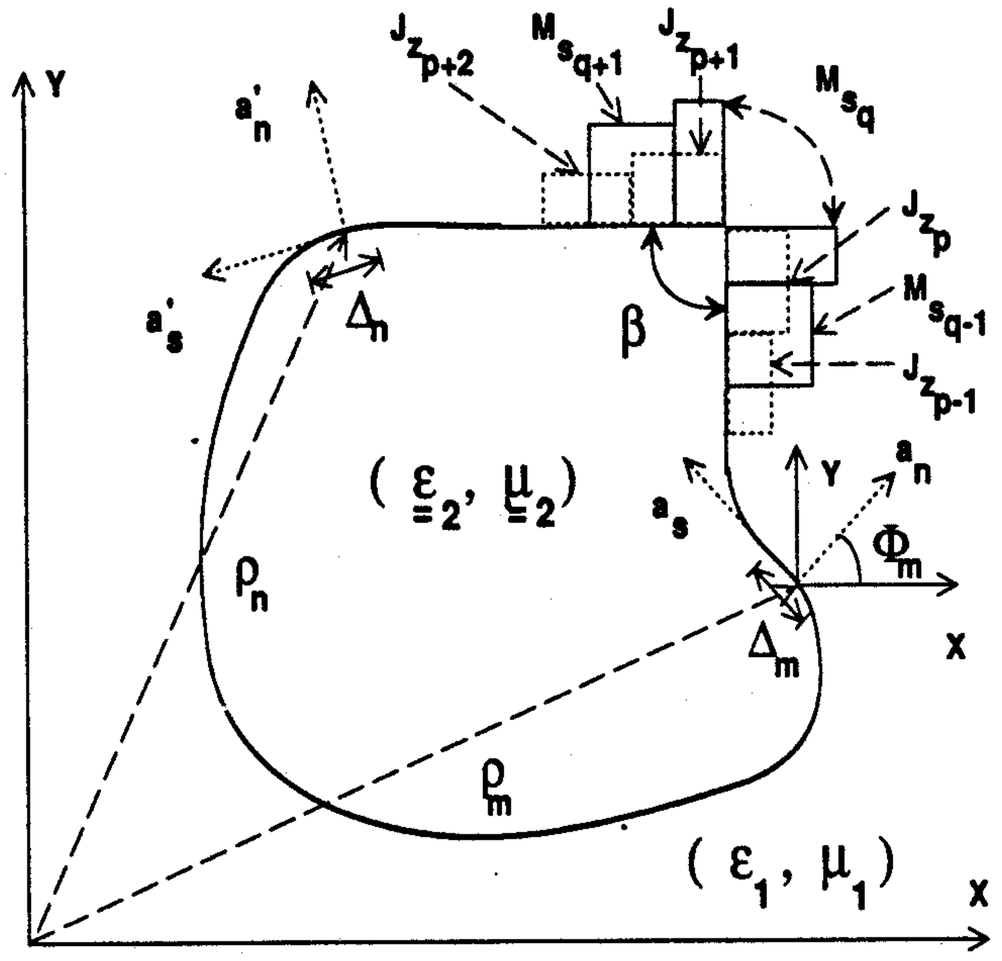

FIGURE 2: Segmented outermost boundary contour

In order to include the effects of the metallic core into the formulation (i = N), the fields $E_{zi+1}(\mathbf{J}_i$ or $\mathbf{J}_{i+1})$ and $\mathbf{H}_{i+1}(\mathbf{J}_{i+1})$ appearing in equations (10) and (11) must be set equal to zero, for there are no fields inside the perfect conductor. In addition, in equation (11), the quantity $\mathbf{a}_{nN} \times \mathbf{H}_{N+1}(\mathbf{J}_N)$ must also be taken to represent the current $\mathbf{J}_N$, which now will be confined to the surface of the conductor. As a result of these modifications, the presence of the core may be accounted for by a single equivalent electric surface current density alone, thereby reducing (10) and (11) to the following simple forms

$$0 = \{ - E_{zN}(\mathbf{J}_N) + E_{zN}(\mathbf{J}_{N-1}, \mathbf{M}_{N-1}) \}_{CN} \tag{14}$$

$$\mathbf{J}_N = J_{zN}\,\mathbf{a}_z = \mathbf{a}_{nN} \times \{ - \mathbf{H}_N(\mathbf{J}_N) + \mathbf{H}_N(\mathbf{J}_{N-1}, \mathbf{M}_{N-1}) \}_{CN} \tag{15}$$

Obviously, since there is only one unknown, namely the current, $\mathbf{J}_N$, flowing on the surface of the conductor (C_N), one of the equations in the set of (14) and (15) becomes redundant, thereby allowing for the use of either *E*- or *H*-field integral equation in formulating the required CFSIEs. In other words, either one of the two potential representations for the **E** and **H** fields

$$\mathbf{E}_N(\mathbf{J}_N) = - j\omega\,\mathbf{A}_N(\mathbf{J}_N) - \nabla\varphi(\rho^e_N) \tag{16}$$

or

$$\mathbf{H}_N(\mathbf{J}_N) = (\underline{\underline{\mu}}_N)^{-1} \cdot (\nabla \times \mathbf{A}_N(\mathbf{J}_N))/\mu_o \tag{17}$$

may be selected to enforce the boundary conditions at the conductor surface. Although it plays no role in TM scattering, the integral representation for the electric scalar potential φ is now defined as the dual of ψ, which is given by equation (5).

The choice of whether *E*- or *H*-field integral equation is employed in the resulting CFSIEs is quite subjective, and is primarily dictated by the desired degree of numerical simplicity; namely, by the ease with which either (16) or (17) can be incorporated into the solution algorithm. To generate results presented in this paper, the *E*-field integral equation was used to represent the fields which are setup by the electric current flowing on the metallic core. However, at all internal boundaries, equations (10) and (11) were used instead, thereby accounting for the presence of all remaining anisotropic layers composing the shielding structure. In order to reduce the surface integral equations for the coated scatterer into their matrix form, a similar approach to that discussed for boundary C_1 was implemented here as well. Just as before, appropriately staggered pulse distributions were employed to expand the unknown surface currents **J** and **M** on each boundary. And subsequently, the same set of basis functions were also utilized to test the integral equations on the corresponding boundaries, thereby providing the desired set of final matrix equations.

2.2 TE Scattering

As opposed to an infinite anisotropic medium or a bulk anisotropic object, for coated scatterers some caution must be exercised when invoking the duality principle to obtain the CFSIEs for the TE incidence — even though such equations for the TM case already exist. This is required since the metal core supports two different components of the current $\mathbf{J}_N$, depending on the polarization of the external excitation. The axial component, J_{zN}, will be induced on the conductor surface under TM-polarization, whereas circumferential current (J_{sN}) will be setup for when the excitation is TE polarized. With this in mind, the fields within anisotropic medium may now be stated as

$$\mathbf{H}_{zi}(r) = -j\omega F_{zi}(\mathbf{J}_i) + \mathbf{a}_z \cdot (\underline{\underline{\mu}}_i)^{-1} \cdot (\nabla \times \mathbf{A}_i(\mathbf{J}_i))/\mu_o \tag{18}$$

$$\mathbf{E}_i(r) = -j\omega \mathbf{A}_i(\mathbf{J}_i) - \nabla \varphi_i(\mathbf{J}_i) - (\underline{\underline{\varepsilon}}_i)^{-1} \cdot (\nabla \times \mathbf{F}_i(\mathbf{M}_i))/\varepsilon_o \,, \tag{19}$$

wherein the corresponding integral expressions for the potentials F_{zi}, $\mathbf{A}_i$, and φ_i are now defined to be

$$F_{zi}(r) = \varepsilon_o/4j \int_{C_i} \gamma_{ei} (\varepsilon_{xx}\varepsilon_{yy})_i^{-1/2} M_{zi}(r') \left(H_o^{(2)}(k_{aei}R_{ei}) \right) ds' \tag{20}$$

$$\mathbf{A}_i(r) = (\mu_o\mu_{zz})_i/4j \int_{C_i} \gamma_{ei} (\varepsilon_{xx}\varepsilon_{yy})_i^{-1/2} \left(\underline{\underline{\varepsilon}}_i^{-1} \cdot \mathbf{J}_i(r') \right) \left(H_o^{(2)}(k_{aei}R_{ei}) \right) ds' \tag{21}$$

$$\varphi_i(r) = 1/(j4\varepsilon_o) \int_{C_i} (\varepsilon_{xx}\varepsilon_{yy})_i^{-1/2} \rho_i^e(r') \left(H_o^{(2)}(k_{aei}R_i) \right) ds' \,, \tag{22}$$

which, simply, are the duals of A_{zi}, $\mathbf{F}_i$, and ψ_i, respectively. Parameters k_{aei}, γ_{ei}, and R_{ei} appearing in equations (20) through (22) may be obtained from (6) and (7) by the replacement of all ε's with μ's, and correspondingly with every μ replaced by ε.

In order to obtain the CFSIEs for treating coated scatterers exposed to plane wave incidence (TE), the boundary conditions on the tangential fields must be enforced at every interface. Equations (10) and (11), with E_{zi} replaced by H_{zi} and $\mathbf{H}_i$ replaced by $\mathbf{E}_i$, may be employed at each internal boundary, and simplified at C_1 to take into account the excitation and the surrounding free-space into the formulation. The minor changes, required in equation set (12) and (13), stem from the fact that signs on curl expressions for **A** as well as **F** must be reversed, as indicated by relations for H_{zi} and $\mathbf{E}_i$, respectively. The final step in derivation of CFSIEs is to include the presence of the metal core via relations (14) or (15), where once again, numerical simplicity will influence the choice of whether *E*- or *H*-field integral equation will be used.

3. NUMERICAL RESULTS

The various two-dimensional scattering geometries for which numerical results using the CFSIEs have been calculated are displayed in Fig. 3. As illustrated, all structures are excited by a normally incident TM-polarized plane wave. Unless otherwise stated, the frequency of this excitation is 300 MHz, and the free-space propagation constant is denoted by k throughout the discussion of this entire section, i. e., $k = 2\pi/\lambda_o$. For all scatterers, C_1 and C_2 are taken to denote their external and internal contours, respectively. The $C_{1,2} = 0$ value corresponds to $y = 0$ and $x > 0$, i. e., the positive x-axis. Exception to this convention occurs in Figs. 4 and 5, where $s = 0$ denotes the center of the shadow region and $s = 0.5$ is located at the center of the illuminated face of the square.

The first example is that of a bulk anisotropic square. Its electrical side dimension is $ks = 10$ and its medium parameters are given by: $\varepsilon_{zz} = 1.5$, $\mu_{xx} = 2$, and $\mu_{yy} = 1.5$. Results for this cylinder using CFSIEs with vector potentials (i. e., equations (1) and (9)) were previously validated against the FD-TD [5]. There it was found that for J_z the agreement was good everywhere, except for the corner regions. For M_s, however, the results obtained by the two methods did not agree very well in the vicinity of corners as well as on the shadow face of the square. When the same case was repeated with the mixed potential formulation (equations (1) and (2)), the agreement for both J_z and M_s as compared to the FD-TD was improved considerably. But since the CFSIEs with mixed potentials are in a very close agreement with the FD-TD, results calculated via the latter method are omitted here in order to avoid unnecessary cluttering of Figs. 4.

For the reported calculations, carried out based on vector and mixed potential formulations, the electric (J_z) and the magnetic (M_s) equivalent surface currents for the square are displayed in Figs. 4a and 4b. Notice that the results for J_z computed via the two methods agree very well along the entire perimeter of the square. On the other hand, the computed values of M_s differ in the vicinity of every corner (i. e., $s = 0.125$ and 0.25) as well as the shadow side of the square. This latter behavior may be directly attributed to the numerical approach used to handle

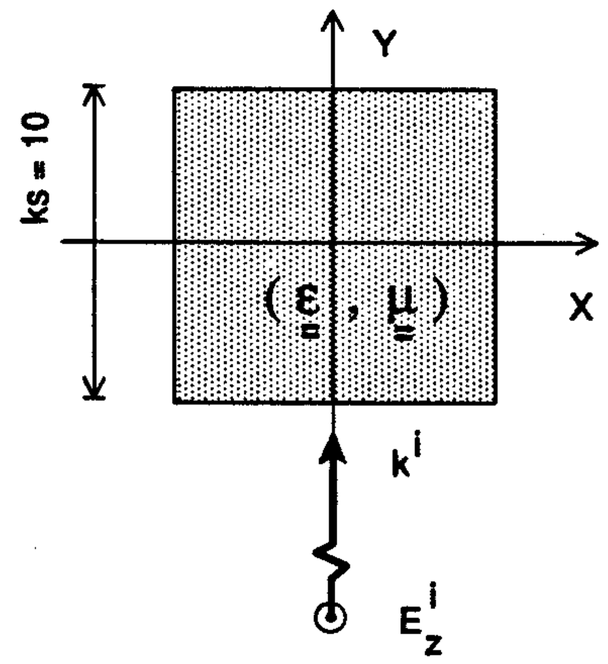

(a) Bulk Anisotropic Square Cylinder

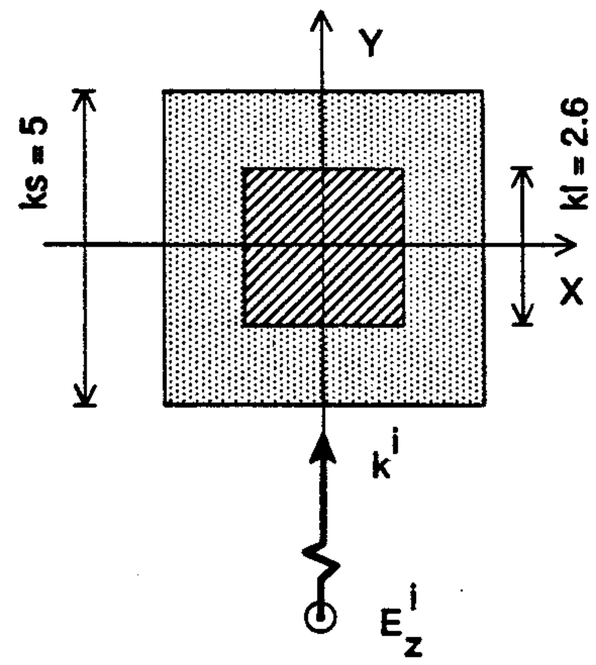

(b) Coated P. C. Square Cylinder

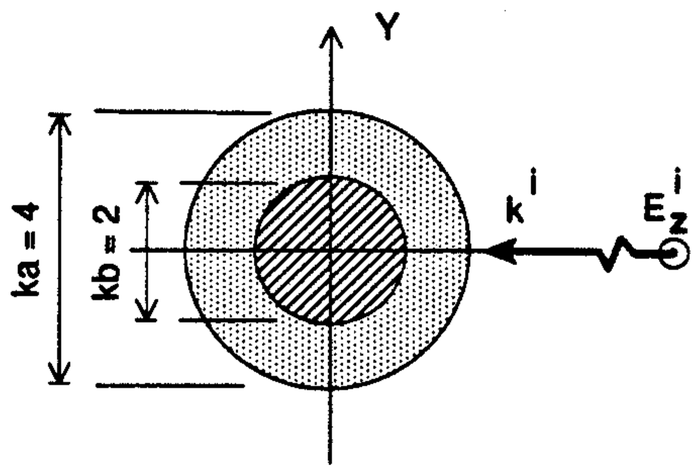

(c) Coated P. C. Circular Cylinder

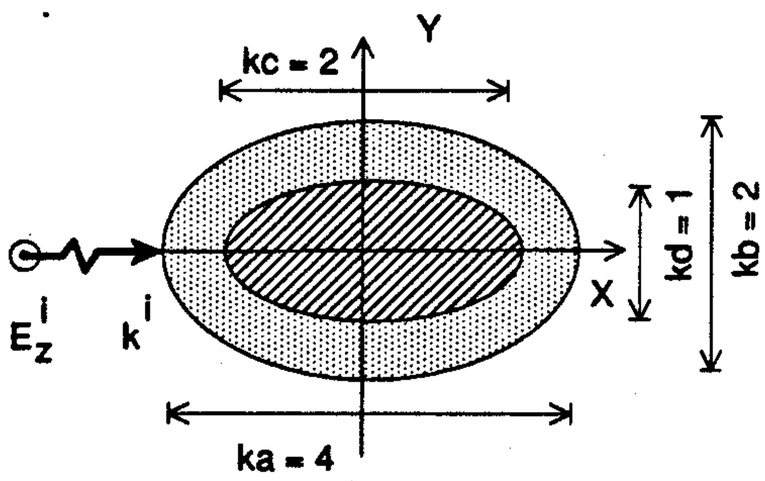

(d) Coated P. C. Elliptic Cylinder

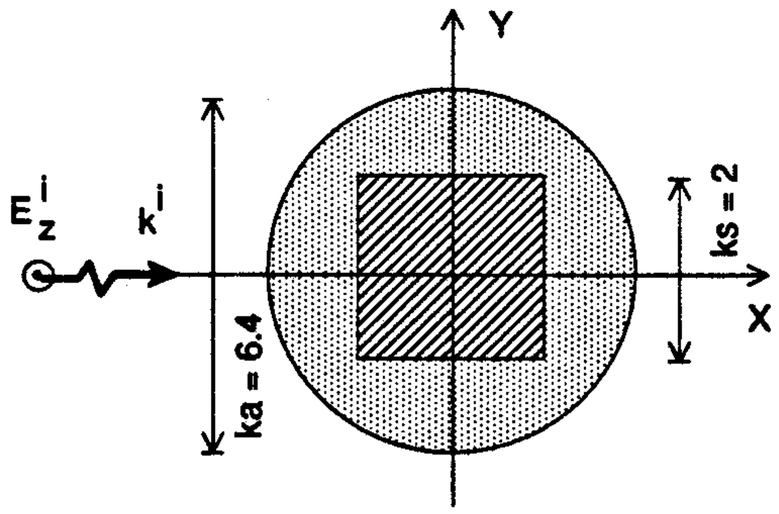

(e) Coated P. C. Square Cylinder

Figure 3: Scattering Geometries

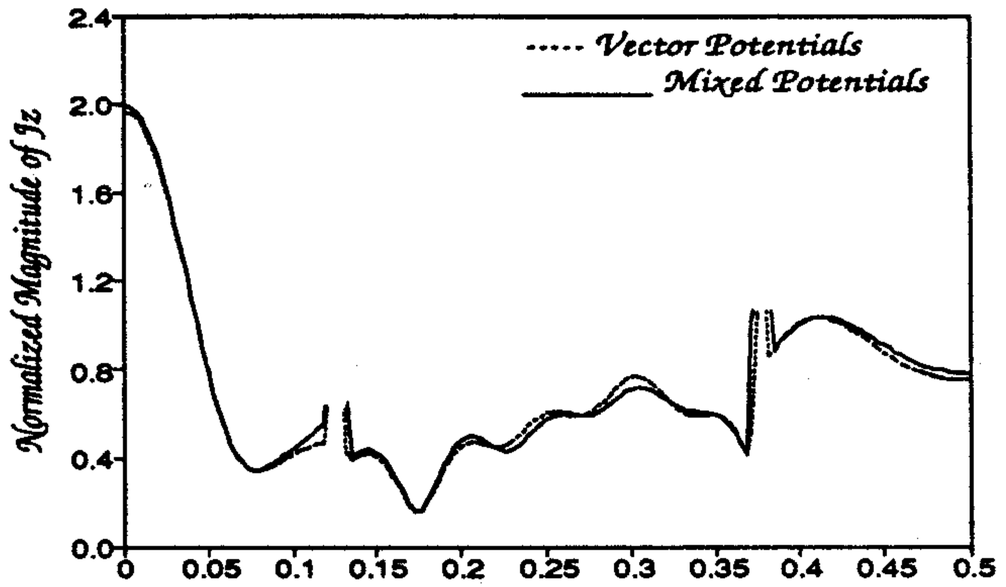

FIGURE 4a: Surface electric current distribution on a bulk anisotropic square.

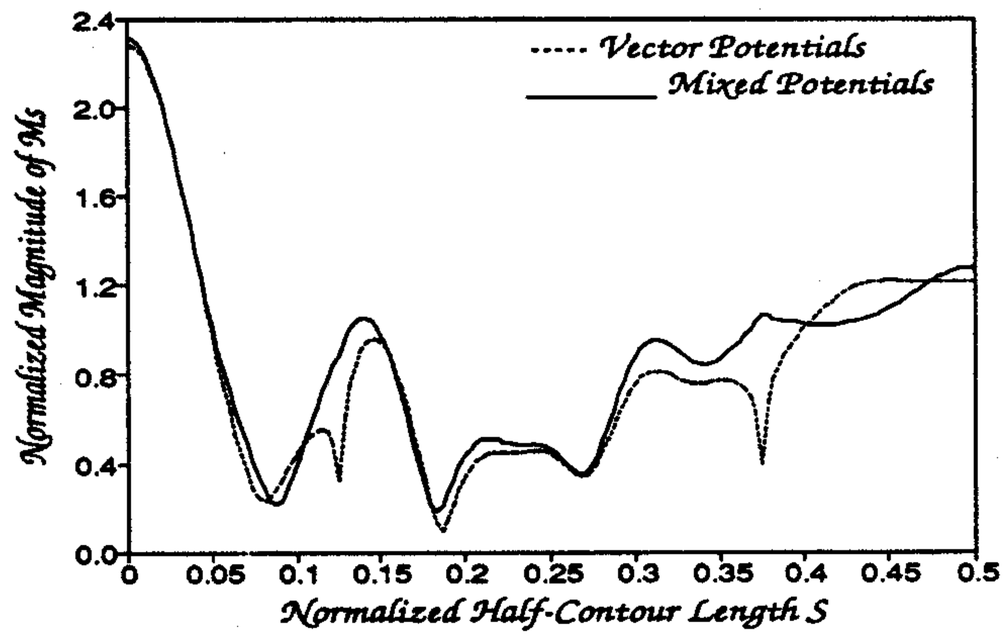

FIGURE 4b: Surface magnetic current distribution on a bulk anisotropic square.

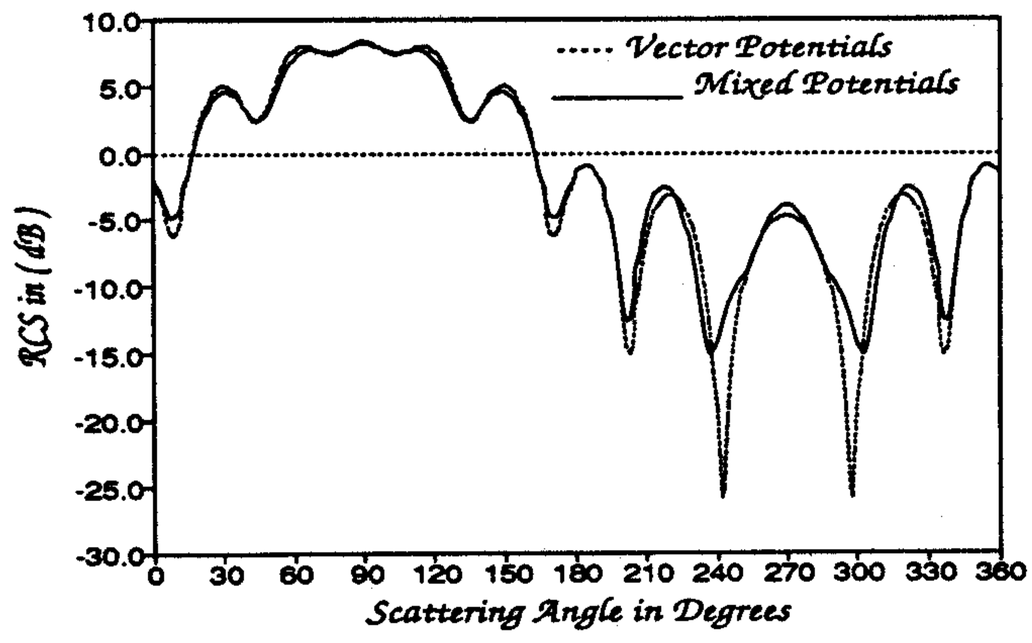

FIGURE 4c: Bistatic RCS of a bulk anisotropic square.

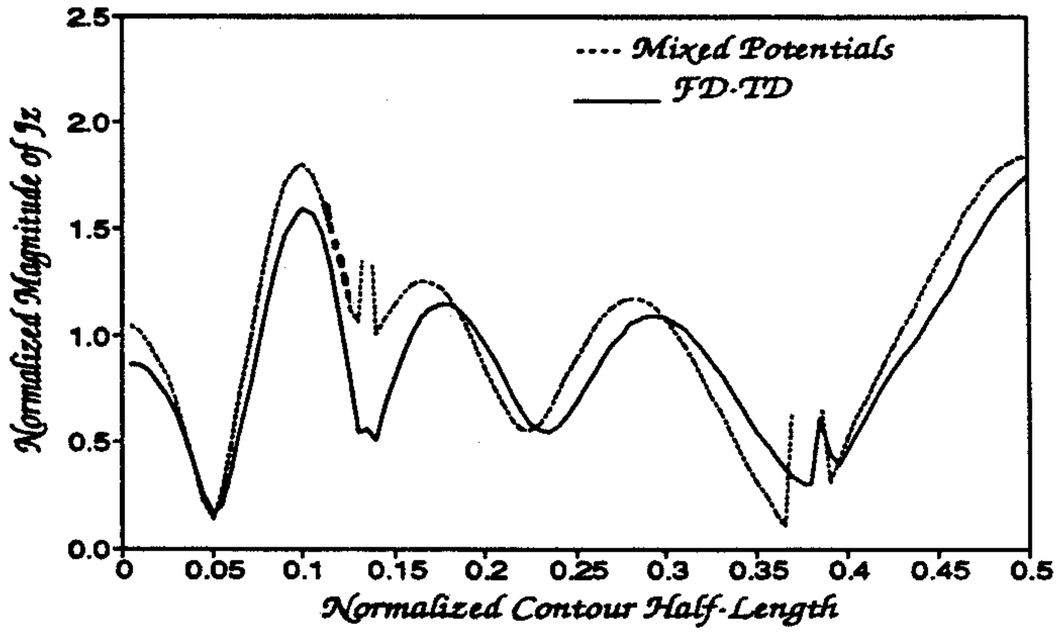

FIGURE 5a: J_z on the coating of a P.C. Square with a square anisotropic layer

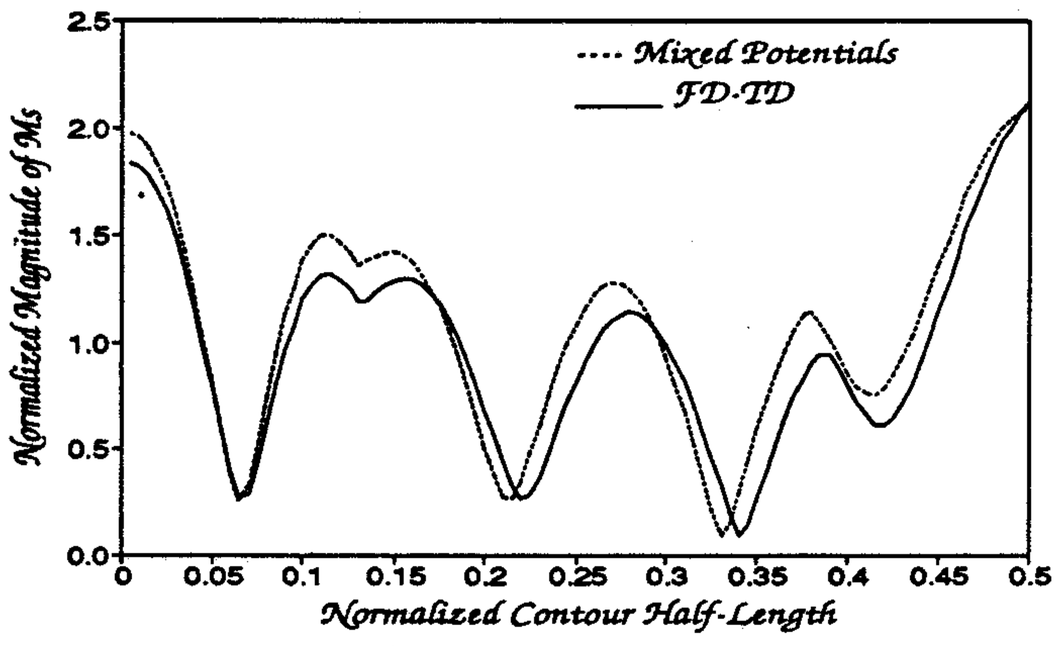

FIGURE 5b: M_s on the coating of a P.C. square with a square anisotropic layer

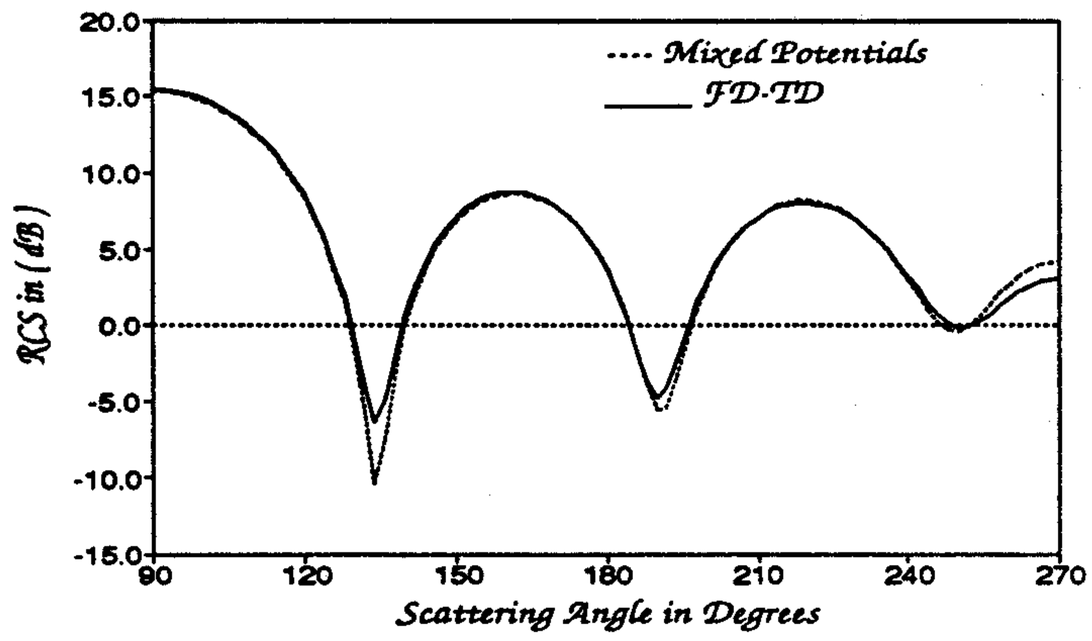

FIGURE 5c: Bistatic RCS of a P.C. square with a square anisotropic layer

singularities at contour discontinuities. Recall that the vector potential approach involves two derivatives of the Green's function. This gives rise to higher order Hankel functions such as $H_2^{(2)}(x)$ in the integrand of the *H*-field equation. Furthermore, this integrand may also be shown to have both odd and even parts as well, which play an important role in the evaluation of principal values [5, equation (10d)].

If the contour is smooth, then the principal value of such integrals may be obtained asymptotically to a very high degree of accuracy [5], [6]. Otherwise, for discontinuous boundaries, principal values must to be evaluated over each M_s half pulse situated on both sides of the bend (see Fig. 2). While this procedure is numerically effective for the even part of the integrand containing $H_2^{(2)}(x)$ as $x \to 0$, for the odd part it is gives undue weight to the difference between the functionals with angular terms which are multiplied by high values of $H_2^{(2)}(x)$ on either side of the discontinuity. As a result, numerical anomalies become apparent in the computed surface currents near the corners of the square when displayed alongside the results obtained via the mixed potential CFSIEs or the FD-TD (see Figs. 4a and 4b). However, despite such discrepancies, the RCS computed by the two methods is not expected to be significantly different. This, of course, is due to the smoothing property of far field integration. And indeed, results displayed in Fig. 4c verify this assertion.

In the next example a perfectly conducting square coated by a single layer of anisotropic material is exposed to an external plane wave excitation. For this case the frequency of the incident field is 150 MHz. The side dimensions of the core and the coating are given by kl = 2.6 and ks = 5, respectively. The medium parameters of the anisotropic coating layer covering the metallic core are $\epsilon_{zz} = 2$, $\mu_{xx} = 2$, and $\mu_{yy} = 4$. The equivalent surface currents on the external contour and the corresponding RCS for this composite structure were calculated via CFSIEs and are compared to those obtained via FD-TD (see Figs. 5). Notice that the surface equivalent current distributions J_z and M_s calculated via the FD-TD and CFSIEs exhibit similar behavior. However, there is a slight disagreement between them which is not unusual and may be attributed to the moderate, as opposed to high, resolution of the FD-TD (50 cells per side on C_1, 26 cells per side on C_2, and 16 cycles). On the other hand, RCS patterns displayed in Fig. 5c show a very close agreement in the numerical results. But this is naturally expected since the far fields are practically insensitive to small perturbations of the surface currents.

As opposed to scattering geometries discussed thus far, results of Figs. 6 and 7 are for objects bounded by smooth contours (see Figs. 3c and 3d). Displayed in Figs. 6a and 6b are the equivalent electric and magnetic current distributions on the surface of the anisotropic circular jacket covering a circular conducting core. The jacket and the core have dimensions of ka = 4 and kb = 2, with the medium properties of the coating layer given by: $\epsilon_{zz} = 1.5$, $\mu_{xx} = 1.5$, $\mu_{yy} = 2.5$, and $\mu_{xy} = 3$. In both cases, a comparison between the vector and the mixed potential approach was made. Calculated results confirm the fact that whenever the scatterer contour is smooth, principal values of all integrals, including those involving $H_2^{(2)}(x)$, may be evaluated with good accuracy. The currents and the corresponding RCS computed via the two versions of CFSIEs are in good agreement with one another, except for some minor discrepancies for M_s. This is due to different convergence rates of the two methods. And since the currents in Figs. 6 were generated using

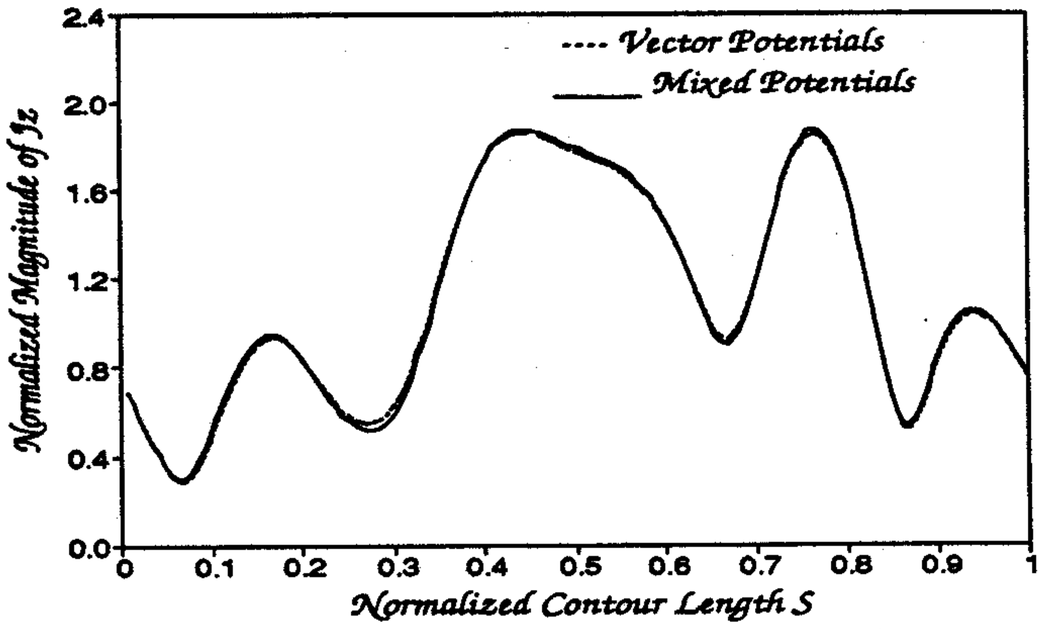

FIGURE 6a: J_z on the coating of a P.C. circle with a circular anisotropic layer

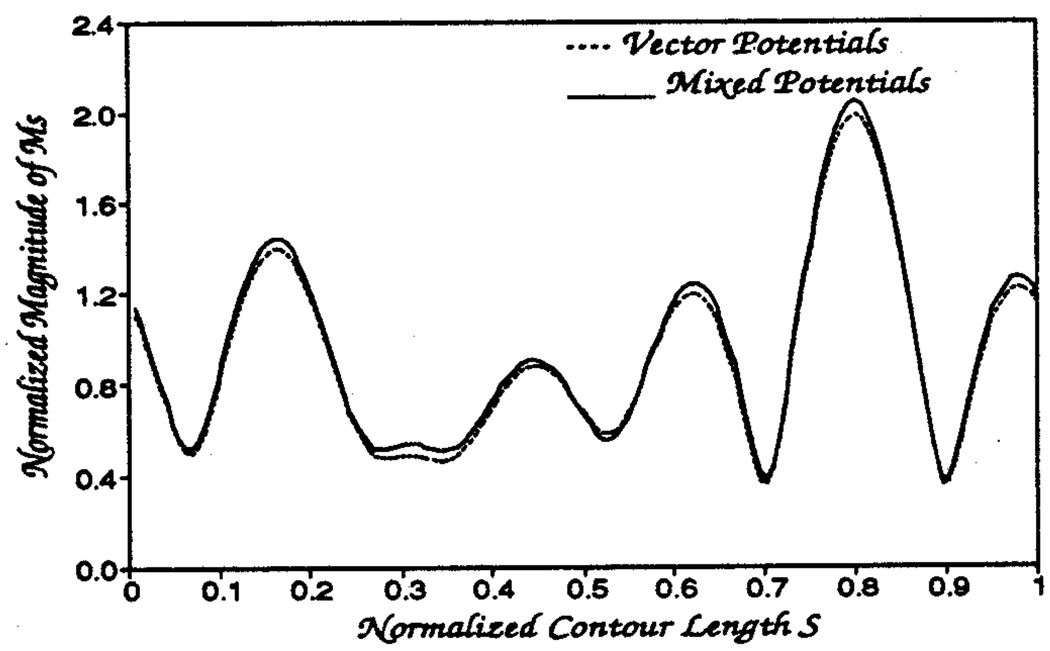

FIGURE 6b: M_s on the coating of a P.C. circle with a circular anisotropic layer

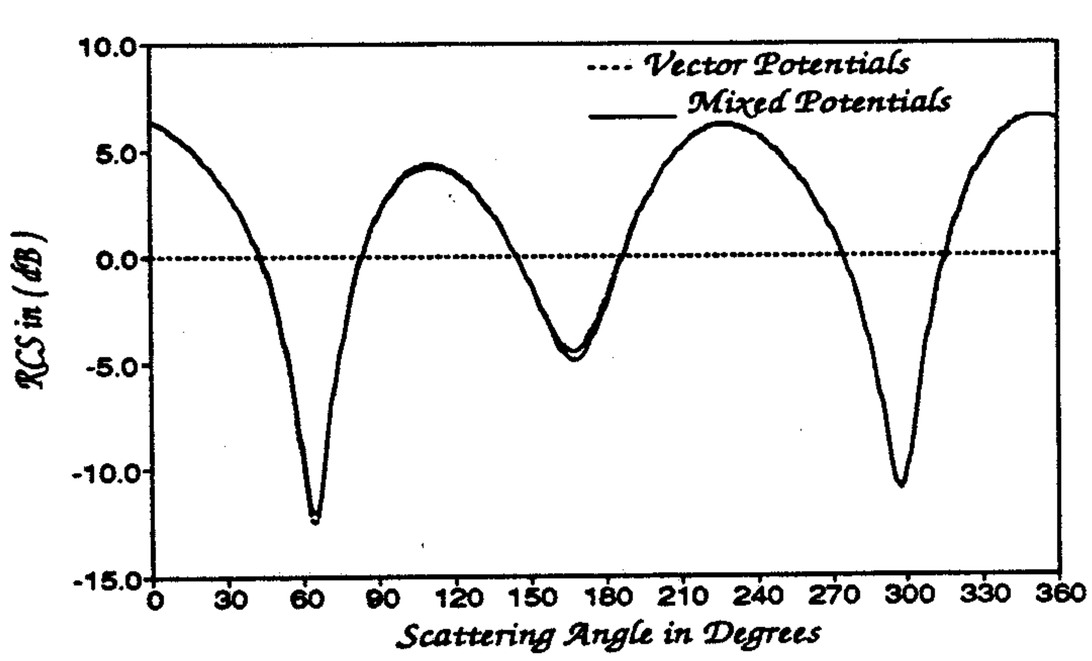

FIGURE 6c: Bistatic RCS of a P.C. circle with a circular anisotropic layer

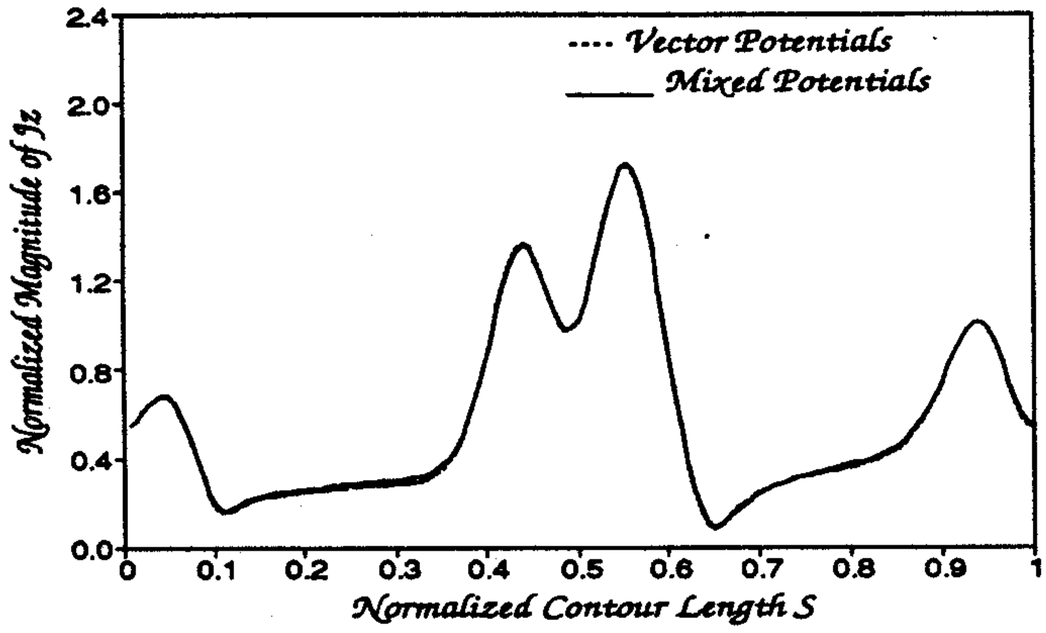

FIGURE 7a: J_z on the coating of a P.C. ellipse with an elliptic anisotropic layer

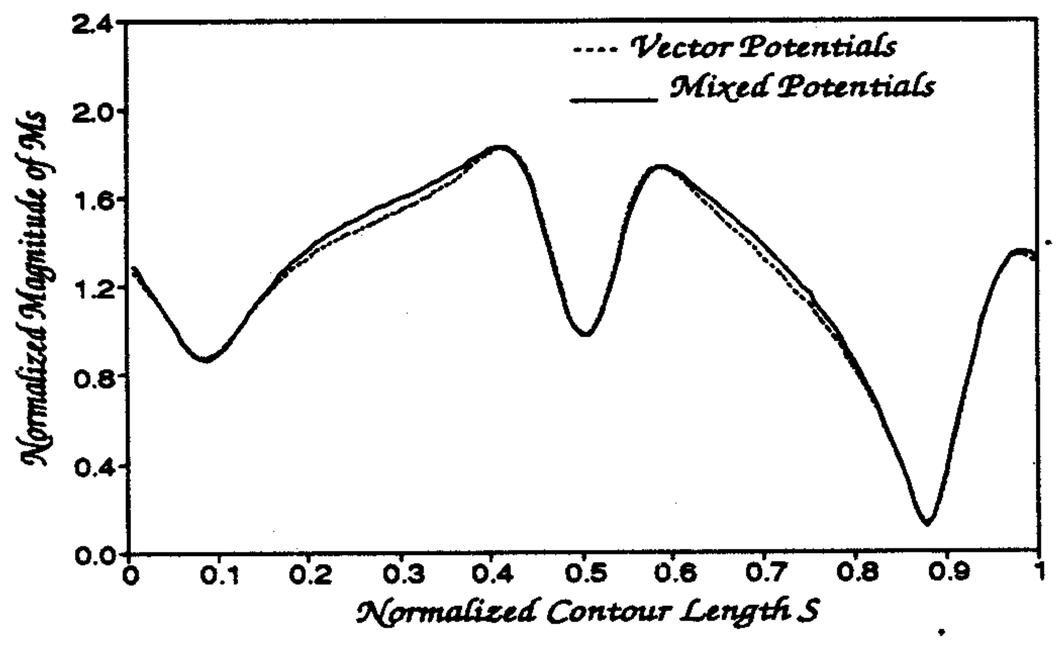

FIGURE 7b: M_s on the coating of a P.C. ellipse with an elliptic anisotropic layer

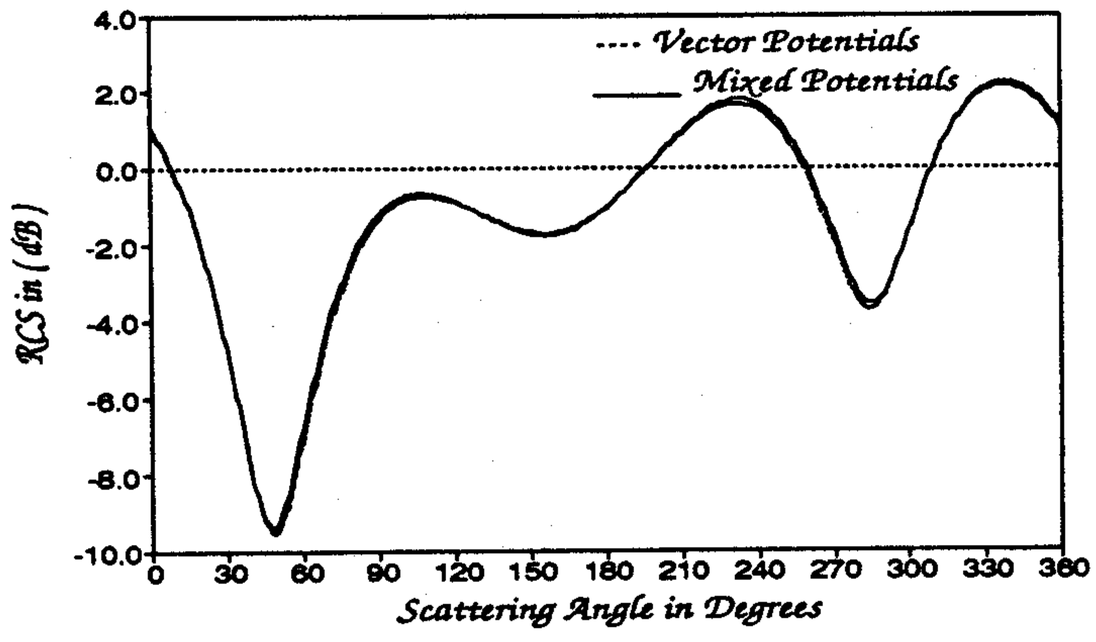

FIGURE 7c: Bistatic RCS of a P.C. ellipse with an elliptic anisotropic layer

the same number of unknowns, it is natural to expect that the two approaches will yield slightly dissimilar results.

Note that in contrast to the first two scatterers whose tensors are diagonal, for coated objects with asymmetric $\underline{\underline{\varepsilon}}$ and $\underline{\underline{\mu}}$, the symmetry about the direction of excitation ceases to exist. Therefore, in Figs. 6 through 9, the surface currents had been plotted along the entire perimeter of each scatterer, whereas in Figs. 4 and 5 the same was done along the contour half-length only.

The next example involves an elliptic conducting core and an elliptic coating layer shown in Fig. 3d. Electrical dimensions of the core and the jacket for this composite structure are $kd = 1$, $kc = 2$ and $kb = 2$, $ka = 4$, respectively. Material properties of the jacket are same as those of the clad circular cylinder. The currents on the external boundary and the RCS for the elliptical scatterer were once again computed using vector as well as mixed potentials, and are presented in Figs. 7. As for the clad circular cylinder, the calculated results are in a good agreement.

A scatterer combining both smooth and discontinuous bounding surfaces was considered for the numerical solution as well. A perfectly conducting cylindrical square core was covered by an anisotropic layer having a circular external boundary (see Fig. 3e). The anisotropic coating material is characterized by the same tensor elements used for elliptic and circular clad cylinders. The side dimension of the core is $ks = 2$ and the normalized diameter of the jacket is $ka = 6.4$. Illustrated in Fig. 8a are the surface current distributions J_z and M_s on the external contour C_1. The corresponding electric current distribution on the surface of the conducting core, C_2, is shown in Fig. 8b. Notice that the current is singular near the edges of the square. This behavior of J_z is well known for conductors imbedded in free-space. But as can be seen from Fig. 8b, such behavior of the electric current near surface discontinuities of metallic objects is also present for conductors imbedded inside the anisotropic medium. And, finally, the calculated RCS for this scatterer is presented in Fig. 8c.

To illustrate applicability of CFSIEs to TE scattering by coated objects, the surface currents and the RCS were calculated for a perfectly conducting clad circular cylinder as well. The medium parameters of the anisotropic shield were taken as $\mu_{zz} = 1.5$, $\varepsilon_{xx} = 1.5$, $\varepsilon_{yy} = 2.5$, and $\varepsilon_{xy} = 3$ with same electrical dimensions as those depicted in Fig. 3c. The magnitudes of currents M_z and J_s on the external layer are now displayed in Fig. 9a, while magnitude of J_s on the metallic core is plotted in Fig. 9b. The corresponding RCS of the composite structure was also calculated, and it appears in Fig. 9c.

4. CONCLUSION

Combined-field surface integral equations were applied to scattering by coated two-dimensional metallic objects. The method was shown to be applicable to coatings as well as the metal cores of arbitrary shape, including surface discontinuities. In addition, the coating material was allowed to have homogeneous anisotropic tensor properties. It was also demonstrated that the CFSIE approach is simple to implement numerically. As illustrated by numerous examples, for such

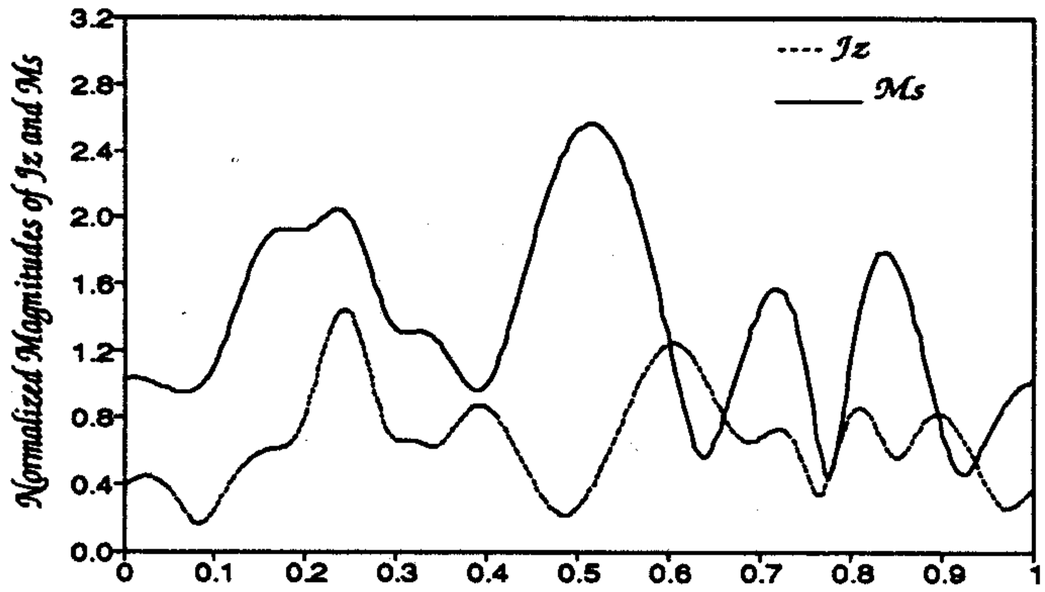

FIGURE 8a: J_z and M_s on the circular coating layer (C_1) of a P.C. Square

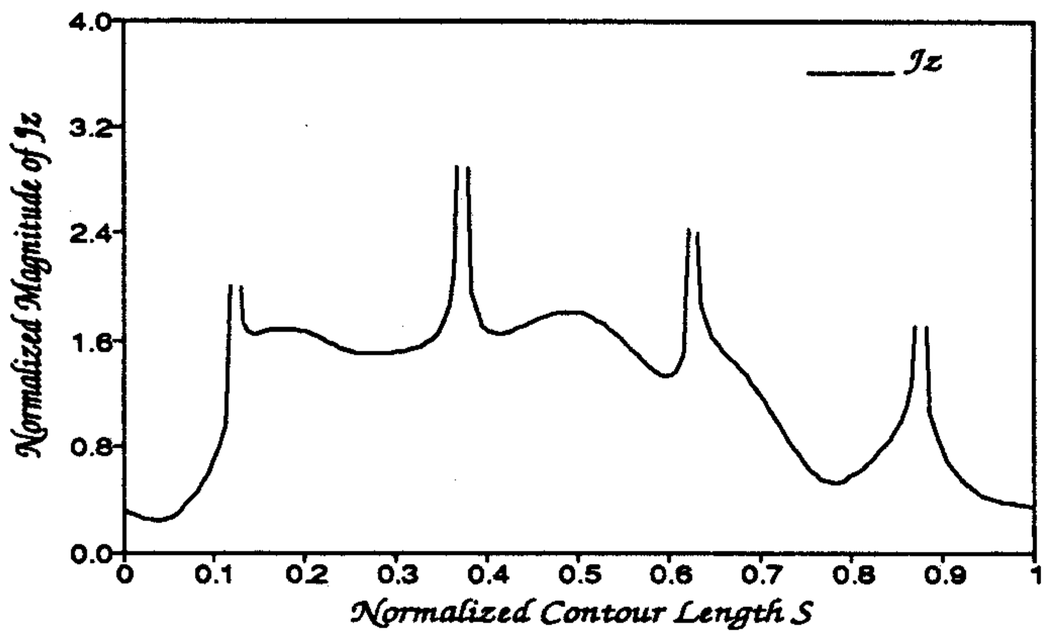

FIGURE 8b: J_z on the core of a P.C. square (C_2) with a circular coating layer

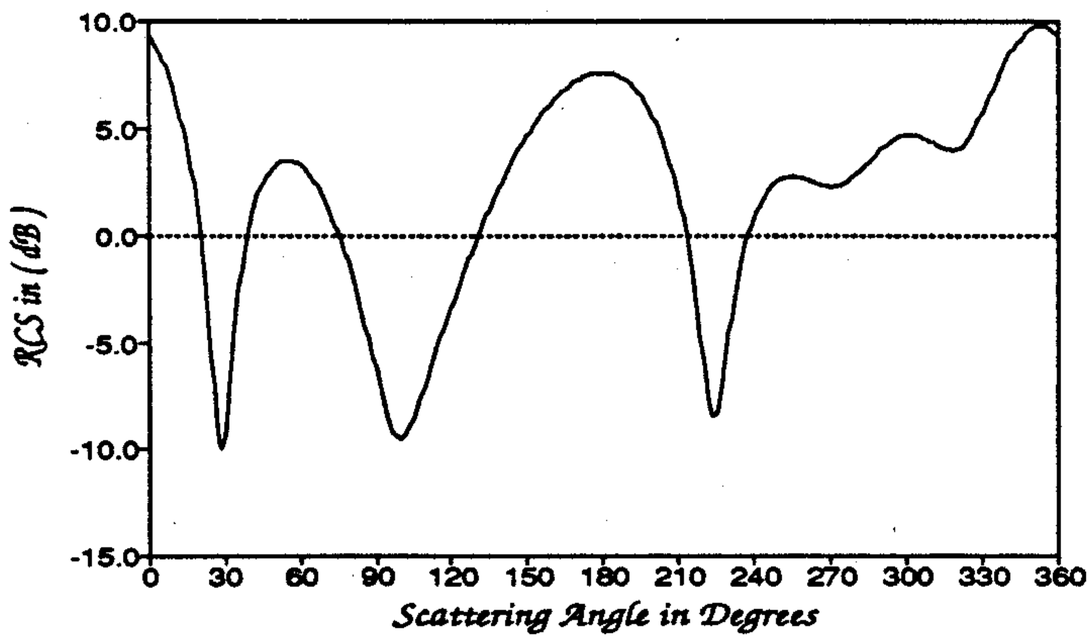

FIGURE 8c: Bistatic RCS of a P.C. square with a circular coating layer

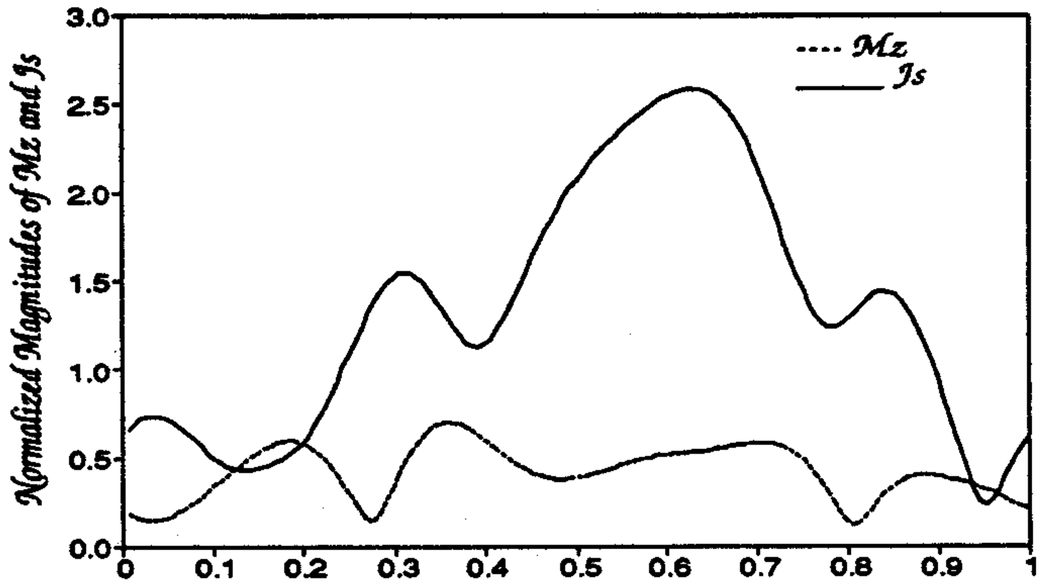

FIGURE 9a: M_z and J_s on the circular coating layer (C_1) of a P.C. circle

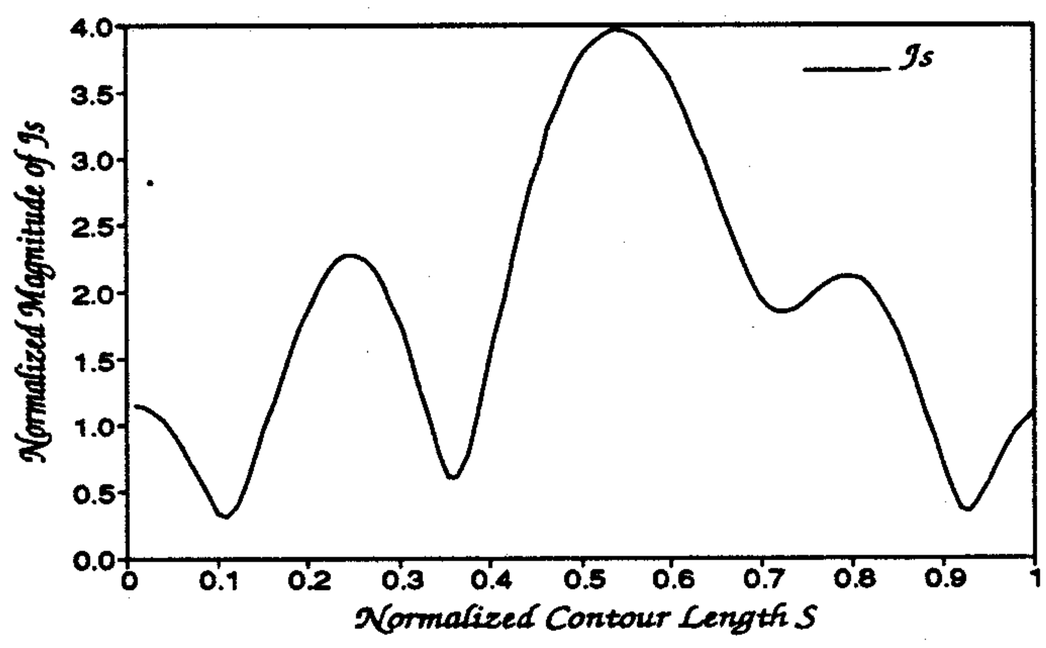

FIGURE 9b: J_s on the core of a P.C. circle (C_2) with a circular coating layer

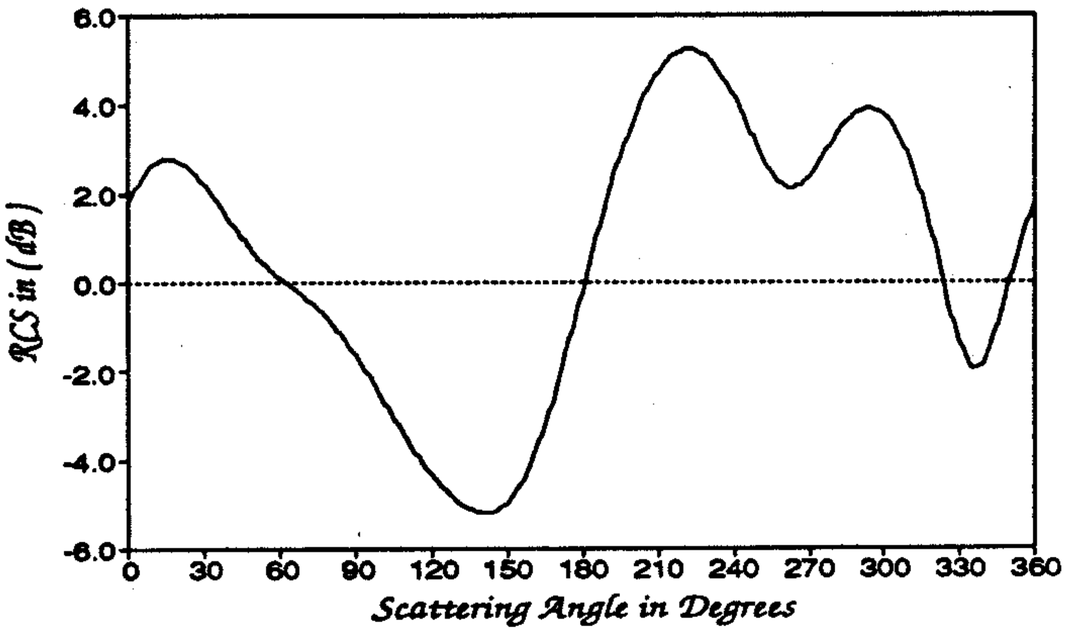

FIGURE 9c: Bistatic RCS of a P.C. circle with a circular coating layer

coated scattering geometries the surface integral equation method yields good results when compared to other numerical methods such as the FD-TD. From the calculated results it was also concluded that for anisotropic scatterers it is more beneficial to work with mixed potentials in the CFSIEs as opposed to vector potentials only. In this manner, numerical difficulties present in evaluating singular portions of integrals containing higher orders of the Green's function are completely avoided.

REFERENCES

[1] Graglia R. D. and Uslenghi P. L. E., Electromagnetic Scattering from Anisotropic Materials, Part I: General Theory, *IEEE Trans. on Antennas and Prop.*, vol. AP-32, no. 4, pp. 867-869, Aug. 1984.

[2] Graglia R. D. and Uslenghi P. L. E., Electromagnetic Scattering from Anisotropic Materials, Part II: Computer Code and Numerical Results in Two-Dimensions, *IEEE Trans. on Antennas and Prop.*, vol. AP-35, no. 2, pp. 225-232, Feb. 1987.

[3] Wu R. B. and Chen C. H., Variational Reaction Formulation of Scattering Problem for Anisotropic Dielectric Cylinders, *IEEE Trans. on Antennas and Prop.*, vol. AP-34, no. 5, pp. 640-645, May 1986.

[4] Beker B. and Umashankar K. R., Analysis of Electromagnetic Scattering by Arbitrarily Shaped Two-dimensional Anisotropic Objects: Combined Field Surface Integral Equation Formulation, *Electromagnetics*, vol. 9, no. 2, pp. 215-229, April 1989.

[5] Beker B., Umashankar K. R., and Taflove A., Numerical Analysis and Validation of the Combined Field Surface Integral Equations for Electromagnetic Scattering by Arbitrarily Shaped Two-dimensional Anisotropic Objects, *IEEE Trans. on Antennas and Prop.*, vol. AP-37, no. 12, pp. 1573-1581, Dec. 1989.

[6] Beker B., Analysis of Electromagnetic Scattering by Arbitrarily Shaped Anisotropic Objects Using Combined Field Surface Integral Equation Formulation, *Ph. D. Dissertation*, University of Illinois at Chicago, Chicago, Illinois, May 1988.

[7] Taflove A., Review of the Formulation and Applications of the Finite-Difference Time-Domain Method for Numerical Modeling of Electromagnetic Wave Interactions with Arbitrary Structures, *Wave Motion*, vol. 10, no. 6, pp. 547-582, Dec. 1988.

[8] Graglia R. D., Uslenghi P. L. E., and Zich R. S., Moment Method with Isoparametric Elements for Three-Dimensional Anisotropic Scatterers, *Proc. of the IEEE*, vol. 77, no. 5, pp. 750-760, May 1989.

[9] Umashankar K. R., Numerical Analysis of Electromagnetic Wave Scattering and Interaction Based on Frequency-Domain Integral Equation and Method of Moments Techniques, *Wave Motion*, vol. 10, no. 6, pp. 493-525, Dec. 1988.

[10] Monzon J. C., On a Surface Integral Representation for Homogeneous Anisotropic Regions: Two-Dimensional Case, *IEEE Trans. on Antennas and Prop.*, vol. AP-36, no. 10, pp. 1401-1406, Oct. 1988.

[11] Graglia R. D. and Uslenghi P. L. E., Anisotropic Layered Absorbers on Cylindrical Structures, *Electromagnetics*, vol. 7, pp. 117-127, 1987.

[12] Massoudi H., Damaskos N. J., and Uslenghi P. L. E., Scattering by a Composite and Anisotropic Circular Cylindrical Structure: Exact Solution, *Electromagnetics*, vol. 8, no. 1, pp. 71-83, Jan. 1988.

[13] Monzon J. C., Electromagnetic Scattering by Metallic Structures Coated with a Rotationally Invariant Anisotropic Medium, *Proc. SPIE*, vol. 927, pp. 220-225, 1988.

[14] Stinson D. C., *Intermediate Mathematics of Electromagnetics*, Chapter 6, Prentice-Hall: Englewood Cliffs, NJ, 1976.

[15] Naiheng Y. and Harrington R. F., Electromagnetic Coupling to an Infinite Wire Through a Slot in a Conducting Plane, *IEEE Trans. on Antennas and Prop.*, vol. AP-31, no. 2, pp. 310-316, March 1981.

[16] Umashankar K. R., Taflove A., and Beker B., Calculation and Experimental Validation of Induced Currents on Coupled Wires in an Arbitrarily Shaped Cavity, *IEEE Trans. on Antennas and Prop.*, vol. AP-35, no. 11, pp. 1248-157, Nov. 1987.